Available online at www.sciencedirect.com
SCIENCE DIRECT
Journal of Sound and Vibration 296 (2006) 23–45
JOURNAL OF SOUND AND VIBRATION
www.elsevier.com/locate/jsvi

Assessment of structural damage using operational time responses and finite element simulation

H.M. Ngwangwa, P.S. Heyns*, F. Van Tonder

Dynamics Systems Group, Department of Mechanical and Aeronautical Engineering, University of Pretoria, Pretoria, 0002, South Africa

Received 18 March 2005; received in revised form 24 October 2005; accepted 24 January 2006
Available online 27 April 2006

Abstract

This paper presents a damage detection technique based on operational response monitoring. The technique utilizes finite element and linear elastic fracture mechanics (LEFM) analyses. The main novel feature of this technique is its ability to identify structural damage completely. The technique is based on monitoring the changes in internal data variability measured by a test statistic χ_0^2 value. Structural normality is assumed when the χ_{0m}^2 value calculated from a fresh set of measured data falls inside the limits prescribed by a threshold value $\chi_{0\mathrm{TH}}^2$. The extent of damage is quantified by matching the χ_{0m}^2 value calculated from the measured data with the corresponding χ_{0p}^2 values predicted by using a benchmark finite element model. The use of χ_0^2 values has been found to provide better sensitivity to structural damage than the natural frequency shift technique. The findings are illustrated in the case of a numerical case study of a simulated steel cantilever beam and an experimental cantilever beam. The analysis done on the numerical study showed that the sensitivity of the proposed technique ranged from three to 1000 times as much as the sensitivity of the natural frequencies. The results obtained from a laboratory structure showed that the extent of damage and the remaining service life could be accurately assessed up to a crack size corresponding to 0.55 of the material's thickness. It was observed that this crack size corresponded to the limiting crack size for the applicability of linear elastic fracture mechanics theory.

1. Introduction

The identification of structural damage is often regarded as a hierarchy of four levels [1]:

- Level 1: Detecting that damage is present in the structure.
- Level 2: Determining the geometric location of the structural damage.
- Level 3: Quantifying the severity of structural damage.
- Level 4: Predicting the remaining service life of the structure.

Many techniques have been developed for identifying structural damage, based on monitoring the global vibration responses [2]. Most of these detection techniques monitor the changes in modal properties, such as the natural frequencies, damping loss factors and mode shapes. These techniques mainly identify damage at Levels 1 and 2 and, when a structural model is used, Level 3 may be attained [3,4].

*Corresponding author. Tel.: +2712 4202432; fax: +2712 3625087.
E-mail address: stephan.heyns@up.ac.za (P.S. Heyns).

0022-460X/$ - see front matter © 2006 Elsevier Ltd. All rights reserved.
doi:10.1016/j.jsv.2006.01.062

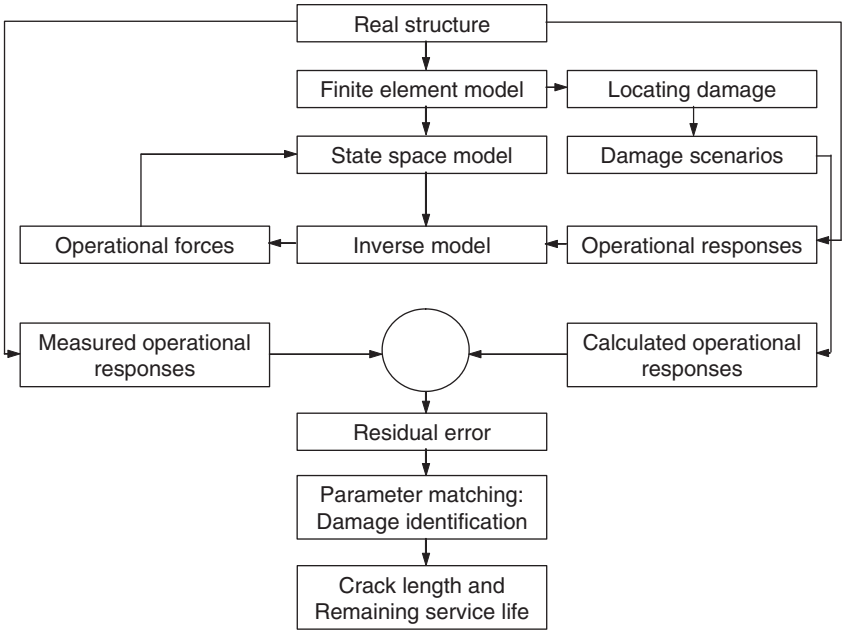

Fig. 1. A flow chart summarizing the damage detection technique.

The recent literature indicates that more efficient algorithms based on advanced statistical analysis tools and artificial intelligence schemes have been developed to assist in damage identification [5–13]. These techniques mainly address the problems of detection efficiency and reliability. Consequently, little effort has been made to develop techniques which can identify all four levels of structural damage.

The technique presented here draws together the analyses of structural dynamics and linear elastic fracture mechanics in order to develop a technique for identifying all four levels of structural damage. In designing the present technique, the assumption made is that the structure cracks by tensile mode under plane strain conditions. As a result, the crack is expected to grow in a straight path through the material thickness normal to the plane of the opening tensile load. This assumption permits the modelling of structural damage by the changes in crack length. Crack branching has not been considered.

In addition to the above assumption about applied loads, the assumption is made that boundary constraints, joints and couplings are maintained in their initial state, i.e. varying load effects have not been considered.

The proposed identification procedure is summarized in a flow chart shown in Fig. 1.

The outline of the technique shown in Fig. 1 indicates that an inverse model is determined from a finite element model (FEM) using time-domain-based model inversion techniques [14]. Then the measured operational responses from the real structure are applied to the inverse model to calculate the operational forces. These forces are applied to the FEM to identify stress 'hot spots' whose locations on the real structure are considered to be the likely locations for damage. Different damage scenarios are then conceived at the identified locations. The operational responses and remaining service life are predicted for each damage scenario. The predicted responses are statistically treated to yield test statistics denoted as χ^2_{0p} values, which are matched to those calculated from the measured operational responses denoted as χ^2_{0m} values. The remaining life that corresponds to the closest match to a predicted response estimates the remaining service life of the beam.

2. Theory

The dynamics of a discrete mechanical system may be given by Eq. (1) [15]

$$\mathbf{M}\ddot{\mathbf{x}}(t) + \mathbf{C}\dot{\mathbf{x}}(t) + \mathbf{K}\mathbf{x}(t) = \mathbf{f}(t), \tag{1}$$

where $\mathbf{M}$, $\mathbf{C}$ and $\mathbf{K}$ are the $N \times N$ mass, damping and stiffness matrices respectively; and $\mathbf{f}(t)$ and $\mathbf{x}(t)$ are the $N \times 1$ force and response vectors respectively.

In the state-space form, Eq. (1) may be written as

$$\dot{\underline{\mathbf{X}}} = \mathbf{E}\,\underline{\mathbf{X}} + \mathbf{d}, \tag{2}$$

where

$$\underline{\mathbf{X}} = \begin{Bmatrix} \mathbf{x}(t) \\ \dot{\mathbf{x}}(t) \end{Bmatrix},$$

$$\mathbf{E} = \begin{bmatrix} \mathbf{0} & \mathbf{I} \\ -\mathbf{M}^{-1}(\mathbf{K}) & -\mathbf{M}^{-1}(\mathbf{C}) \end{bmatrix}$$

and

$$\mathbf{d} = \begin{Bmatrix} \mathbf{0} \\ \mathbf{M}^{-1}\mathbf{f}(t) \end{Bmatrix}.$$

A numerical integration scheme may be employed to solve Eq. (2).

Structural damage is presumed to change the mass, stiffness and damping matrices of the system. However, for a structure with surface cracking, where disintegration (resulting in mass loss) is not likely and changes in the system damping are not considered, damage may be assumed to affect only the stiffness matrix of the system. The influence of the crack on the system's stiffness matrix is localized in the elements where the cracks are located. In the present paper, a special cracked beam finite element is used for modelling the structural damage. The element allows the direct manipulation of the stiffness matrix by a crack ratio parameter $\bar{a}$, which is defined as $\bar{a} = a/H$, where a is the length of the crack and H is the thickness of the material [16]. Fig. 2 shows a diagram of the damage modelling.

In order to relate structural damage to changes in the time responses, Eq. (2) may be differentiated in respect of crack length a as follows:

$$\frac{\partial \dot{\underline{\mathbf{X}}}}{\partial a} = \frac{\partial(\mathbf{E}\,\underline{\mathbf{X}})}{\partial a} + \frac{\partial \mathbf{d}}{\partial a}. \tag{3}$$

Since the mass matrix, damping matrix and force vector are not affected by changes in crack length, Eq. (3) yields Eq. (4) upon further simplification.

$$\frac{\partial \dot{\underline{\mathbf{X}}}}{\partial a} = \mathbf{E}\frac{\partial \underline{\mathbf{X}}}{\partial a} + \mathbf{E}'\,\underline{\mathbf{X}}, \tag{4}$$

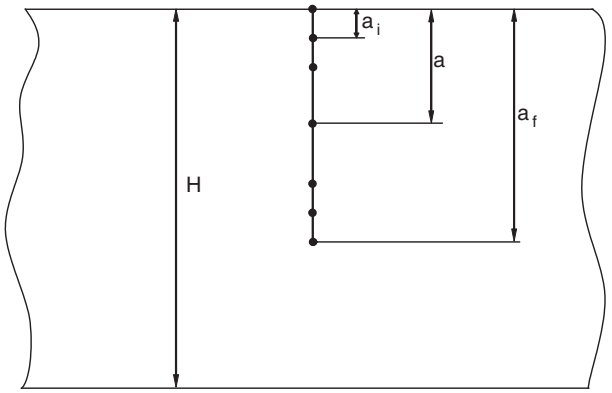

Fig. 2. A schematic diagram showing damage represented by crack ratios.

where

$$\mathbf{E}' = \begin{bmatrix} \mathbf{0} & \mathbf{0} \\ -\mathbf{M}^{-1}\dfrac{\partial \mathbf{K}}{\partial a} & \mathbf{0} \end{bmatrix}.$$

The forward finite difference method [17] may be used to compute $\partial \mathbf{K}/\partial a$ thus

$$\frac{\partial \mathbf{K}}{\partial a} = \frac{\mathbf{K}(a_{i+1}) - \mathbf{K}(a_i)}{a_{i+1} - a_i}, \tag{5}$$

where $i = 0, 1, 2, \ldots$

Then the calculated change in the state vector $\underline{\dot{\mathbf{X}}}$ with respect to the change in crack length a can be represented by a sensitivity function $\mathbf{s}$, which may be given by

$$\mathbf{s} = \frac{\partial \underline{\dot{\mathbf{X}}}}{\partial a}. \tag{6}$$

The time response at crack length a_{i+1} may be approximated by using a first-order Taylor series expansion as

$$\underline{\dot{\mathbf{X}}}(a_{i+1}) = \underline{\dot{\mathbf{X}}}(a_i) + \mathbf{s}\delta a, \tag{7}$$

where

$$\delta a = a_{i+1} - a_i.$$

2.1. Determining the test statistics

The time responses estimated by Eqs. (2) and (7) are treated statistically to determine their variations from the response of the undamaged structure. The residues between these estimated time responses $\underline{\dot{\mathbf{X}}}$ and the undamaged structure's responses $\underline{\dot{\mathbf{X}}}_u$ are input into a statistical model which is based on the hypotheses that test internal data variability. The hypotheses test the equality between the variances determined from the residues of the estimated time responses and some reference residue vector. This reference residue vector could ideally be a null vector but to avoid some numerical problems, 0.1% of the undamaged structure's response was arbitrarily chosen. Thus given the estimated time responses $\underline{\dot{\mathbf{X}}}_1, \underline{\dot{\mathbf{X}}}_2, \underline{\dot{\mathbf{X}}}_3, \ldots, \underline{\dot{\mathbf{X}}}_k, \ldots, \underline{\dot{\mathbf{X}}}_n$, their residues may be calculated and the following hypotheses used to test the internal variability [18]:

$$H_0^2 : \sigma_u^2 = \sigma_1^2 = \sigma_2^2 = \sigma_3^2 = \cdots \sigma_k^2 \cdots = \sigma_n^2, \quad H_1^2 : \sigma_u^2 \neq \sigma_k^2, \sigma_{k+1}^2, \ldots, \sigma_n^2, \tag{8}$$

where σ_u^2 and σ_k^2 are the variances for the residues of the reference vector and the kth time response. It may be worth noting that in the H_1^2 hypothesis, where only one or a few intermediate time responses happen to satisfy the test, it could be due to some exceptional causes like, sensor error, noise effects, variations in boundary conditions, load fluctuations, etc.

Bartlett's test [18] provides a procedure for testing the variability of variances among different data sequences through a test statistic χ_0^2 value. The test statistic χ_0^2 is computed using Eq. (9):

$$\chi_0^2 = 2.3026\frac{q}{c}, \tag{9}$$

where

$$q = (R - r)\log_{10} S_p^2 - \sum_{k=1}^{r}(n_k - 1)\log_{10} S_k^2,$$

$$c = 1 + \frac{1}{3(r-1)}\left(\sum_{k=1}^{r}(n_k - 1)^{-1} - (R - r)^{-1}\right)$$

and

$$S_p^2 = \frac{\sum_{k=1}^{r}(n_k - 1)S_k^2}{R - r},$$

where r is the number of data sequences being considered, R is the total number of data units in the r sequences, n_k is the number of data units in the kth data sequence. S_p^2 is the combined sample variance of the r data sequences, including the reference sample variance, S_u^2. S_k^2 is the variance of the kth response.

The test statistic χ_0^2 value is compared with a threshold $\chi_{0\mathrm{TH}}^2$ value, which may be established from the expected disturbances in the system. Since a 1% disturbance level above the response of the undamaged structure was observed to produce detectable changes in the test statistic value, it was used in this work for the calculation of the threshold value. Accordingly, if $|\chi_0^2| > |\chi_{0\mathrm{TH}}^2|$, the null hypothesis is rejected because the time responses are not equal and therefore there is an abnormality in the test data.

2.2. Determining the remaining service life

In LEFM theory, it is assumed that there is a small plastic zone $2r_y$ at the tip of a crack and that this zone is surrounded by a field called the region of K-dominance. This assumption yields the following expressions for the size of the plastic region [19,20]:

$$2r_{y\sigma} = \frac{1}{\pi}\left(\frac{K}{\sigma_y}\right)^2, \quad 2r_{y\varepsilon} = \frac{1}{3\pi}\left(\frac{K}{\sigma_y}\right)^2, \tag{10}$$

where the subscripts σ and ε represent the states of plane stress and plane strain respectively, and σ_y is the material yield strength. K is the stress intensity factor which depends on the loading, crack size, crack shape and geometric boundaries. The stress intensity factor K is given by [19]

$$K = f(g)\sigma\sqrt{\pi a} \tag{11}$$

where σ is the remote stress applied to the component, a is the crack length and $f(g)$ is the correction factor that depends on specific crack geometry.

In order to apply LEFM theory, the plastic zone has to be smaller than all the distances from the crack tip to any material boundaries. Therefore the expression for the applicability of LEFM theory may be given by [20]

$$\begin{aligned} &a, (b-a), h > \frac{4}{\pi}\left(\frac{K}{\sigma_y}\right)^2 \quad \text{for plane stress,} \\ &t, a, (b-a), h > 2.5\left(\frac{K}{\sigma_y}\right)^2 \quad \text{for plane strain,} \end{aligned} \tag{12}$$

where the distances are as shown in Fig. 3.

The rate of crack growth may be given by the Paris relationship as

$$\frac{\mathrm{d}a}{\mathrm{d}N} = C(\Delta K)^m, \tag{13}$$

where C, m and ΔK are the crack growth coefficient, the crack growth exponent and the stress intensity range respectively. The stress intensity range is given by

$$\Delta K = f(g)\Delta\sigma\sqrt{\pi a}, \tag{14}$$

where $\Delta\sigma$ is the effective remote stress range applied to the component.

Thus Eq. (13) can be used for obtaining the crack propagation life to failure N_f:

$$N_f = \int_{a_i}^{a_f} \frac{\mathrm{d}a}{C(\Delta K)^m} \tag{15}$$

where the integration limits a_i and a_f represent an initial and a final crack size, respectively. The remaining service life can be determined by subtracting the propagation life at each crack length from the propagation

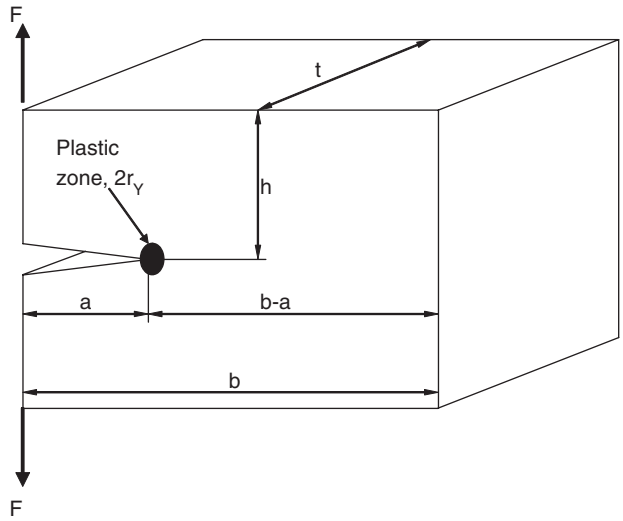

Fig. 3. Distances from crack tip to any material boundaries.

life to failure:

$$\mathrm{RSL}_a = N_f - N_a, \tag{16}$$

where RSL_a denotes the remaining service life at a crack length a.

3. Description of the technique

The full technique comprises the following:

- System modelling and force identification.
- Modelling the structural damage.
- Predicting the responses.
- Identifying the structural damage.

The technique solves the problem of structural damage via the forward problem formulation, in which structural damage (crack length) is determined by comparing measured changes in structural time responses with the predicted changes in time responses. The predicted changes in structural time responses are initially calculated from the known structural damage using the FEM. These changes are benchmarked against the measured changes in the time responses.

3.1. System modelling and force identification

A FEM of the real structural system as given by Eq. (1) is developed. Synthetically generated excitation is applied to the FEM to identify an autoregressive parametric model, which is subsequently converted into a state-space model as given in Eq. (2). The state-space model is then inverted, using time-domain-based techniques.

Then the measured operational responses are applied to the inverse model to calculate, in an offline manner, the operational forces. The identified operational forces are applied to the FEM to identify stress 'hot spots' in the structure. The locations of the stress 'hot spots' in the model are considered to be the likely locations of damage.

3.2. Modelling the structural damage

As mentioned above, structural damage is represented by a crack ratio denoted by $\bar{a}$. Therefore, taking the worst-case scenario as crack ratio a_f/H the crack propagation space (from a virgin state to the worst case) is scaled into convenient damage scenarios, each of which is represented by a crack ratio (Fig. 2). An assumption is made that the crack does not branch but grows linearly and uniaxially. This assumption is basically aligned with fractures under a plain strain state.

Then the Paris law is applied to calculate the remaining life to failure for each of the damage scenarios, using Eqs. (15) and (16). In this way, each damage scenario is characterized by both the crack ratio and the remaining service life.

3.3. Predicting the responses

As shown in Fig. 1, the operational responses are initially predicted at each crack ratio, using the FEM. Then the dynamic sensitivity coefficients given by Eq. (6) are used for fine-tuning the predictions to achieve a better fit with the operational measured responses. The first-order Taylor series expansion of Eq. (7) is employed to estimate the responses.

3.4. Identifying the structural damage

The changes in the operational responses between the undamaged and the damaged structure are monitored by the χ_0^2 values calculated using Eq. (9). These test statistic values are used as damage identification features.

In the following two sections, the technique is verified by means of numerical and experimental case studies.

4. Technique verification: numerical case study

In this case study, a numerical simulation of a steel cantilever beam is presented. The beam is 800 mm long, 40 mm wide and 10 mm thick. Its Young's modulus E, and material mass density ρ, are $207 \times 10^9\,\mathrm{N/m^2}$ and $7810\,\mathrm{kg/m^3}$, respectively. A harmonic force $F(t) = 1.3\,\mathrm{kN}$ at a frequency of 5 Hz is applied at a distance of 200 mm from the fixed end for a duration of 2 s. Fig. 4 depicts a diagram of the structure.

The simulated operational responses were generated from the FEM with a fine mesh. The FEM had to closely approximate the natural mode shapes and frequencies calculated by using exact equations of the beams in transverse vibrations [21]. Fig. 5a indicates that an 80-element FEM satisfied this requirement reasonably well. As a result, this model was used for calculating the simulated operational responses (referred to as pseudo-measured responses) at six different levels of structural damage: 0.0, 0.2, 1.4, 3.3, 4.2 and 5.7 mm crack lengths.

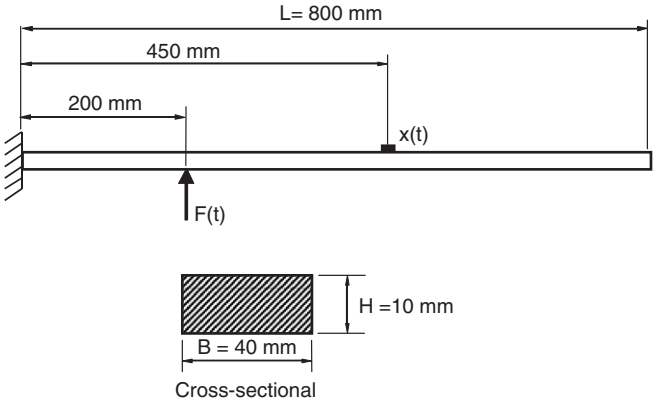

Fig. 4. Schematic diagram of beam structure.

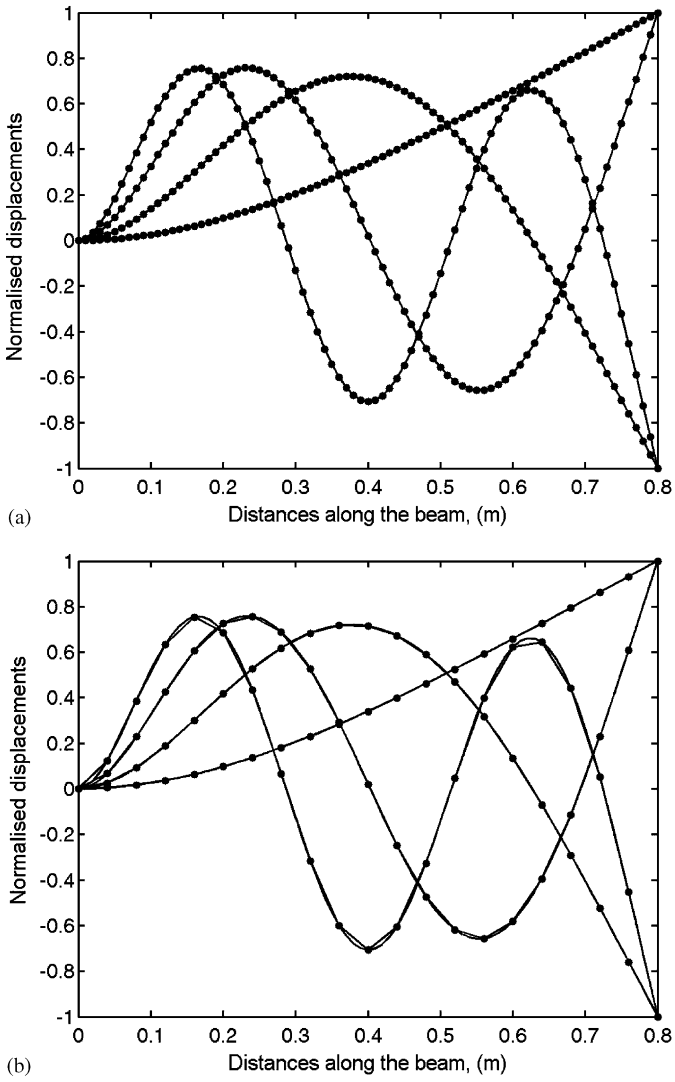

Fig. 5. Fit between mode shapes: (a) 80-element FEM (—•—) and exact solution (——). (b) 20-element FEM (—•—) and exact solution (——).

Subsequently, an attempt was made to identify damage using the pseudo-measured operational responses. To this end, a working FEM of the structural beam was developed. The choice of its mesh density depended on how accurately it approximated the simulated operational response for an undamaged structure. However, the first mode of vibration was the most influential in causing damage because of the volume effect in fatigue cracking (where cracking is more likely as the volume of material subjected to fatigue increases) and the amplitude–frequency relationship in vibrating structures. Therefore the working FEM had to approximate closely at least the first mode of vibration.

4.1. Modelling the beam

The structural beam was modelled in MATLAB 6.1 on a Pentium 4 platform with 1.7 GHz and 256 MB of random access memory (RAM). The Euler–Bernoulli beam elements were used for modelling all the undamaged parts of the structure, whereas the damaged part was modelled by a special cracked-beam element. Fig. 5b indicates that a 20-element FEM is accurate for the first two shapes and frequencies of the flexural bending mode. Similarly, the calculated frequency response functions in Fig. 6, and the acceleration responses

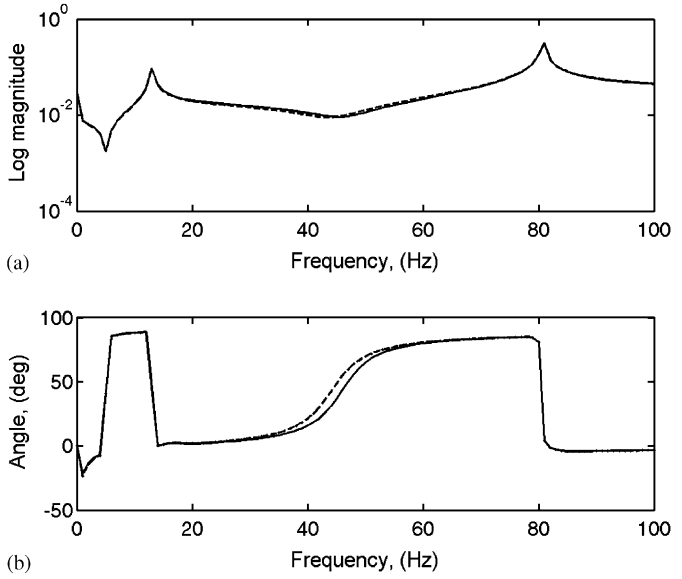

Fig. 6. Frequency response functions for the 20-element (dashed) and 80-element (solid) FEM: (a) acceleration FRF plots and (b) phase angle plots.

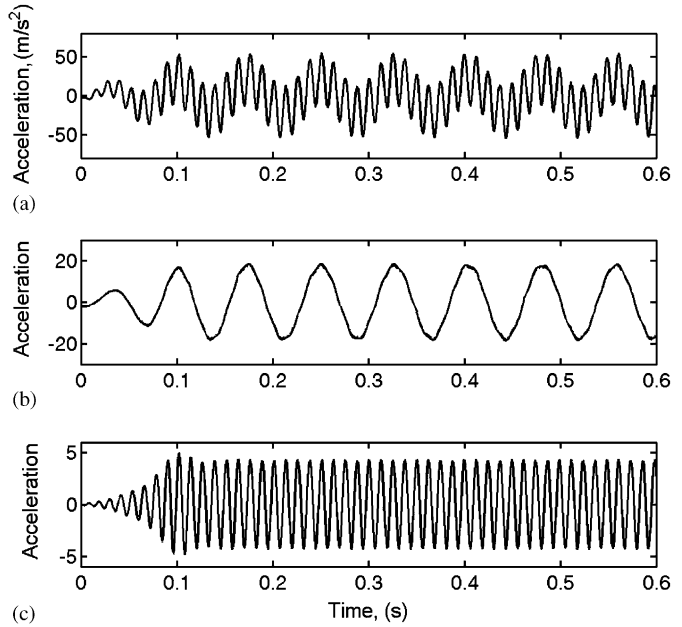

Fig. 7. Fit between acceleration responses at different frequencies—20-element (– · – · ·) and 80-element (——) FEM: (a) In the 10–90 Hz bandwidth, (b) around the first natural frequency, 13 Hz and (c) around the second natural frequency, 81 Hz.

in Fig. 7, show a close correspondence between the 20- and 80-element FEM. For these reasons the 20-element FEM was chosen as the working model.

4.2. Damage scenarios

For the uniform cross-section cantilever beam, the fixed end is the most likely damage location because the stresses are the highest there. Hence the cracked-beam finite element is the first element of the structural FEM.

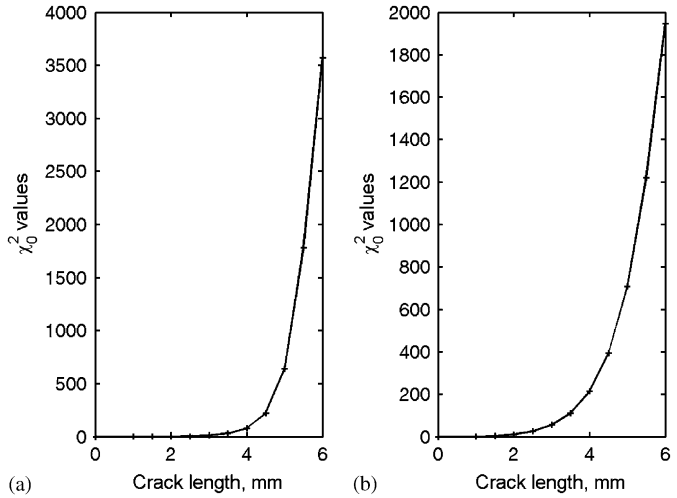

Fig. 8. Predicted test statistic values: (a) χ_0^2 values at first natural frequency and (b) χ_0^2 values at second natural frequency.

Since the crack is located in the middle of this element, its geometric position is 20 mm from the fixed end of the beam.

In this example the damage scenarios have been classified by the following crack ratios: 0.0, 0.1, 0.15, 0.2, 0.25, 0.3, 0.35, 0.4, 0.45, 0.5, 0.55 and 0.6. Since the beam thickness is 10 mm, these crack ratios correspond to crack lengths of: 0.0, 1.0, 1.5, 2.0, 2.5, 3.0, 3.5, 4.0, 4.5, 5.0, 5.5 and 6.0 mm deep through the beam thickness.

The corresponding time responses for the excitation force $F(t)$ given earlier, were calculated for each crack ratio using the 20-element FEM. The responses were band-pass-filtered around the first and second natural frequencies so that proper comparisons could be made with the changes in the corresponding natural frequencies. Then the root square values of the filtered responses were computed and sorted in ascending order to provide a check on normality and data variation. The entire period of 2 s was considered.

Using Eq. (9), Bartlett's test was applied to the root square values calculated above to predict the χ_{0p}^2 values for each damage scenario, where p denotes the prediction. Fig. 8 shows graphs of these values plotted against crack lengths for the first and second natural frequencies. Both plots depict a trend typical of crack propagation behaviour. Therefore the χ_0^2 values quite ably capture the characteristics of crack growth.

At the same time, crack propagation and the remaining service life are computed using Eqs. (15) and (16), respectively. Fig. 9 shows the resulting curves. It was noted that when the crack length reaches the crack ratio of 0.6, the remaining service life (for the crack to penetrate through the remaining 4 mm) is half as much as that required for the material to crack from 0.5 to 0.6 (which is only 1 mm).

4.3. Damage detection

Next the intention was to identify structural damage using the simulated operational responses. The detection scheme computes the χ_{0m}^2 value of the pseudo-measured response signal and matches it to the predicted χ_{0p}^2 values. It yields the crack length that has a χ_{0p}^2 value closest to the computed χ_{0m}^2 value. The subscript m is used here to represent the values calculated from the pseudo-measured responses, but in the case of an actual experiment it would represent the values calculated from the measured responses. Therefore, when the pseudo-measured responses were employed in the detection scheme, they yielded the results shown in Table 1. These were regarded as the initial estimates of the actual damage level.

The resulting initial estimates provided a basis for a more refined estimation of crack length in a sensitivity-based algorithm. The search was initialized from the time responses that corresponded to the estimated crack lengths shown in Table 1. The second-order Taylor series expansion was used with a step size of 0.001 for the crack ratio. The first and second derivatives were calculated numerically, using a central difference scheme. As expected, the truncation of higher-order derivatives in the central difference scheme affected the accuracy of the solution, especially at the end of the time span. In this case, it was noted that for crack ratios of up to 0.45,

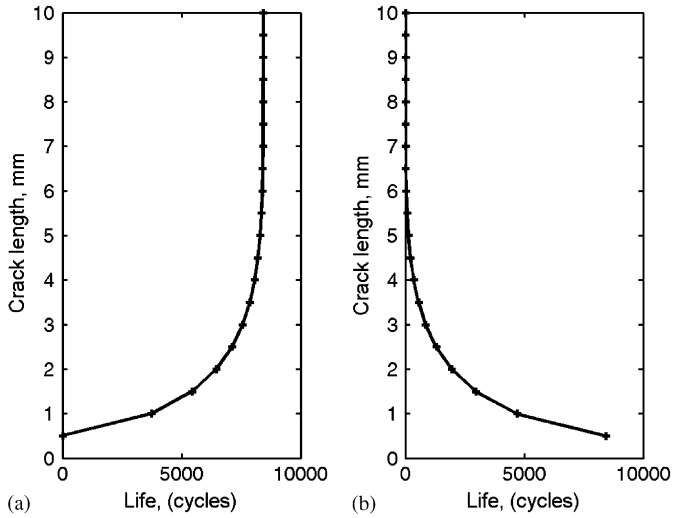

Fig. 9. Predicted propagation and remaining service life curves: (a) propagation life curve and (b) remaining service life curve.

Table 1
Initial estimates of crack lengths and remaining service life

Actual			Estimated			Remaining life (cycles)
Crack	χ_0^2: 13 Hz	χ_0^2: 81 Hz	Crack	χ_0^2: 13 Hz	χ_0^2: 81 Hz	
0.2	0.00	0.00	0.0	0.00	0.00	8438
1.4	0.40	2.40	1.5	0.50	3.20	2981
3.3	19.00	84.30	3.0	11.30	55.30	867
4.2	115.50	273.40	4.0	80.80	213.80	361
5.7	2380.30	1485.70	5.5	1779.10	1220.00	78

more than a third of the data length closely matched the actual responses. Beyond this crack ratio (0.45), higher orders in both the Taylor series expansion and central difference scheme might be required for an accurate prediction of the time responses.

Figs. 10–12 show the correspondence between the initial and final estimates of the acceleration responses, with the actual (pseudo-measured) acceleration responses at each damage level for three selected cases of damage. It was noted that for 0.2, 4.2 and 5.7 mm, the scheme converged after 20 iterations, whereas for 1.4 and 3.3 mm, convergence occurred after 10 backward and 30 forward iterations, respectively. When the products of the number of iterations and step sizes were added to the initial estimates, it was found that convergence took place at exact crack lengths. Consequently the crack lengths were identified with a high degree of accuracy. The corresponding remaining service life can be easily read off from the remaining service life curves shown in Fig. 9.

4.4. Comparison with the changes in natural frequencies

In this section, the proposed technique is compared with the changes in natural frequencies. The changes in the first two natural frequencies are presented in Fig. 13.

Table 2 compares the absolute changes in natural frequencies with the absolute changes in the χ_0^2 values per millimetre of the change in crack length in each damage scenario (from 0.5 to 6 mm). It is observed that at the first natural frequency, the sensitivity of the proposed technique ranged from three times to over 1000 times the sensitivity of the natural frequency shift technique. Around the second natural frequency, the sensitivity ranged from four times to over 200 times that given by the natural frequency shift technique.

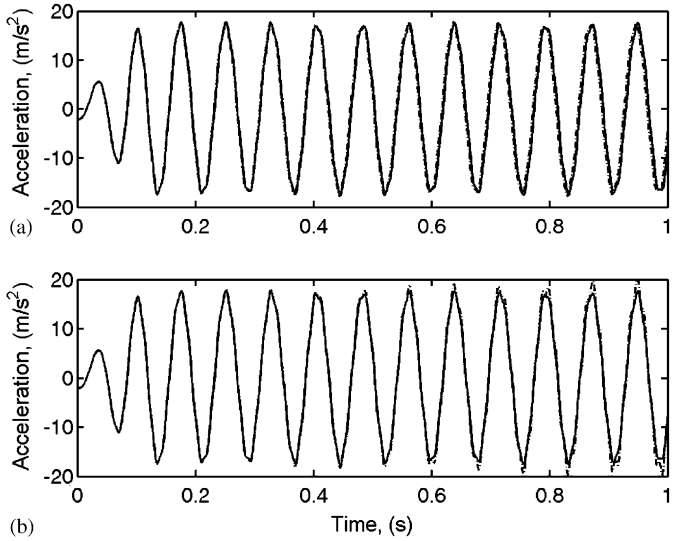

Fig. 10. Initial and final estimates of the acceleration response at 1.4 mm crack length: (a) initial estimate (dashed) and actual (solid) and (b) final estimate (dashed) and actual (solid).

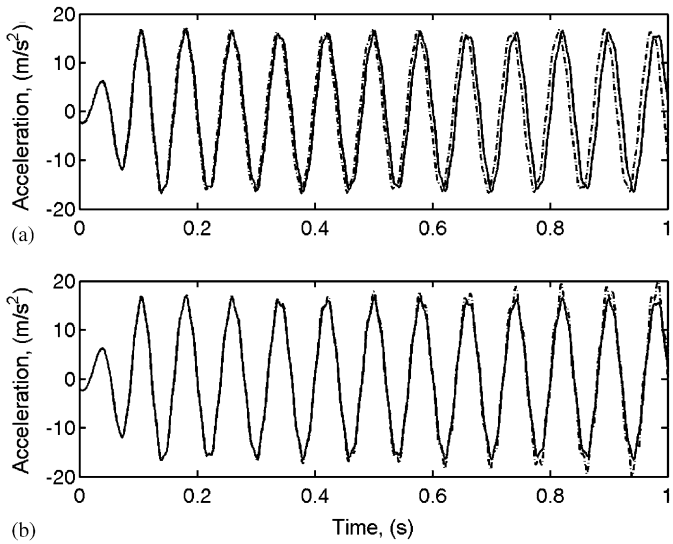

Fig. 11. Initial and final estimates of the acceleration response at 3.3 mm crack length: (a) initial estimate (dashed) and actual (solid) and (b) final estimate (dashed) and actual (solid).

Fig. 14 compares the relative changes in natural frequencies and χ_0^2 values at each crack ratio up to 0.6. The results show that the relative changes in the test statistics values lie above 30%, while those in the natural frequencies are below 20%. Thus the proposed technique is shown to be far more sensitive than the natural frequency shift technique.

5. Technique verification: experimental case study

In the experimental case study, a mild steel beam 1165 mm long, 50 mm wide and 12 mm thick was clamped at one end over a length of 125 mm, leaving a cantilever length of 1040 mm. The beam had the following material and fatigue properties: Young's modulus of elasticity E, 207×10^9 N/m^2, mass density ρ, 7810 kg/m^3,

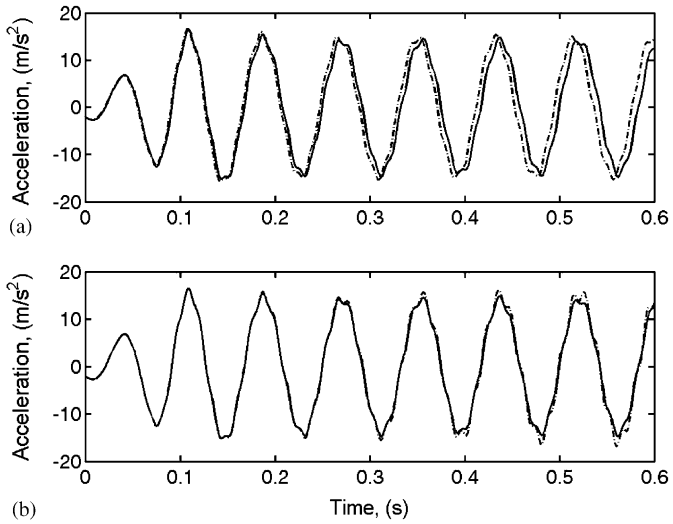

Fig. 12. Initial and final estimates of the acceleration response at 4.2 mm crack length: (a) initial estimate (dashed) and actual (solid) and (b) final estimate (dashed) and actual (solid).

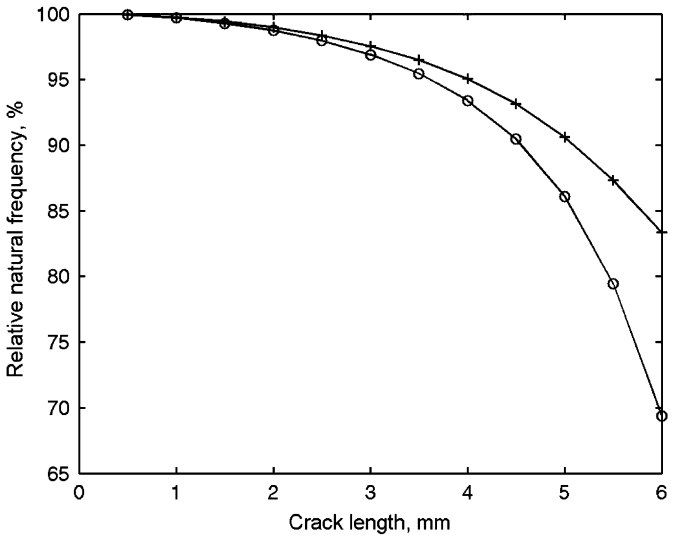

Fig. 13. Relative natural frequency drop for the first (—o—) and second (—+—) natural frequencies.

yield strength σ_y, $658 \times 10^6\,\mathrm{N/m^2}$, crack growth coefficient C, $6.89 \times 10^{-12}\,\mathrm{MPa}\,\sqrt{\mathrm{m}}$ and crack growth exponent m, 3.0 [22]. A 45° v-notch 2 mm in depth was cut at a distance of 40 mm from the fixed point.

Three tests were performed. In Tests 1 and 2, the structure was excited by an initial force of 1.4 kN force at a frequency of 7 Hz. This resulted in a stress level of 177.0 MPa and a strain amplitude of $856.81\,\mu\varepsilon$, which were verified by actual strain gauge measurements [23]. A crack-measuring sensor was placed at a distance of 1 mm below the notch tip so that the total crack-measuring depth was 8.0 mm. The total initial crack length was 3.0 mm.

In Test 3, the excitation was lowered slightly to an initial force of 1.25 kN, which resulted in 158 MPa of stress. The crack sensor was placed 2.0 mm below the notch tip, giving a total initial crack length of 4.0 mm. This enabled measurements of the crack length to be taken up to a total structural thickness of 9.0 mm. In all three tests the beam was excited at a distance of 465 mm from its fixed end.

Table 2
Sensitivity comparisons between test statistic values and natural frequencies

Crack change		Frequency derivatives		χ_0^2 derivatives	
From (mm)	To (mm)	$\lvert\Delta f_n/\Delta a\rvert_{13\ \mathrm{Hz}}$	$\lvert\Delta f_n/\Delta a\rvert_{81\ \mathrm{Hz}}$	$\lvert\Delta\chi_0^2/\Delta a\rvert_{13\ \mathrm{Hz}}$	$\lvert\Delta\chi_0^2/\Delta a\rvert_{81\ \mathrm{Hz}}$
0.5	1.0	0.0623	0.3238	0.20	1.60
1.0	1.5	0.1012	0.5184	0.80	4.80
1.5	2.0	0.1452	0.7336	1.80	14.20
2.0	2.5	0.2008	0.9926	5.20	30.00
2.5	3.0	0.2746	1.3198	14.60	60.00
3.0	3.5	0.3782	1.7466	38.40	112.00
3.5	4.0	0.5298	2.3194	100.60	205.00
4.0	4.5	0.7632	3.0982	282.80	360.40
4.5	5.0	1.1352	4.1342	838.60	628.00
5.0	5.5	1.7302	5.3776	2275.20	1024.00
5.5	6.0	2.6154	6.4510	3579.60	1454.60

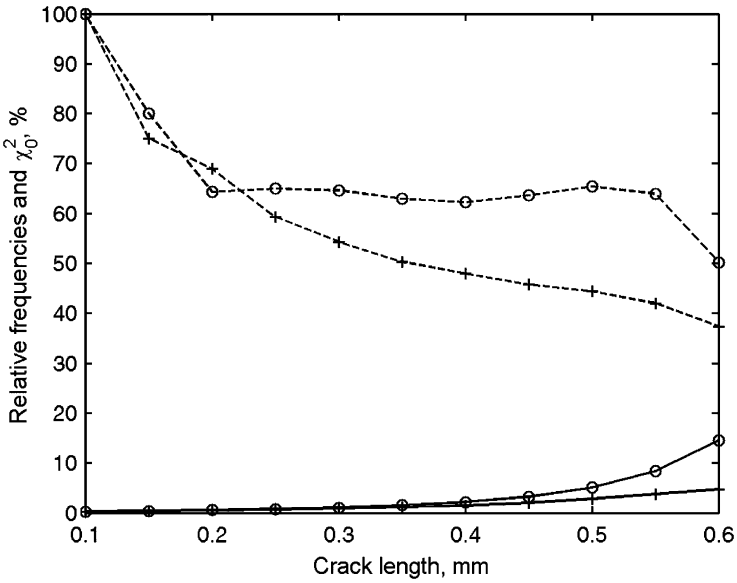

Fig. 14. Comparison of the relative changes in natural frequencies (solid) and test statistics (dashed).

The tests were performed in displacement control using a Zonic® Master Controller. The excitation was externally generated through a CDAS system to provide better control during the actuation period. In all these tests the actuation was performed for durations of 60 s during which measurements were taken for a period of 10 s. The cycles were read from the cycle counter display on the Zonic® Master Controller.

5.1. The measurement system

The data was obtained by using a Spider 8 measurement system through a laboratory desktop computer, as shown in Fig. 15. A 10 mV/g accelerometer, a type Y-series (1-LY11-6/120A) strain gauge and a type RDS22 series crack propagation gauge were used as sensors in the experimental case study.

The crack gauge had 50 grids of resistance circuits spanning a total width of 5 mm. This yielded a measurement resolution of 0.1 mm per grid. It was used for measuring the length of the crack as the crack spread through the material. It operates on the principle that the resistance increases as the growing crack

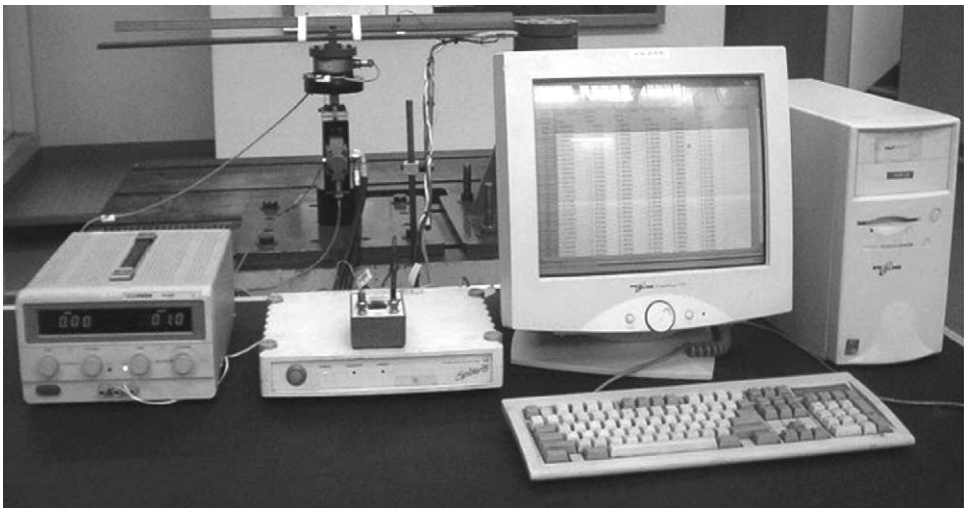

Fig. 15. The measurement system and data acquisition hardware.

breaks the grid. The change in crack length is indicated by the decrease in the voltage measured across a resistor connected in series to it. A supply voltage of 1 V was maintained throughout the testing period.

5.2. Damage scenarios

The undamaged parts of the beam were modelled by 37 Euler–Bernoulli beam elements whereas the damaged part was modelled by the cracked-beam element. The damage scenarios for the FEM were conceived from an initial notch depth of 2 mm to a final total crack length of 7.2 mm. The initial crack length corresponded to a crack ratio of 0.167, whereas the final crack length corresponded to a crack ratio of 0.6.

The remaining service life and χ^2_{0p} values were predicted for each damage scenario and plotted against the crack lengths. The resulting curves were compared with their counterparts from the measured data. The next section presents the correspondence between the predicted curves and the curves obtained from the data measured during the experimental study.

The validity of the LEFM assumptions was also checked for each damage scenario. Fig. 16a shows that the LEFM assumptions made for plane strain and plane stress states are applicable up to 5.5 and 6.7 mm (0.56 crack ratio) crack lengths respectively, in Tests 1 and 2. Consequently there is a transition from a plane strain state to a plane stress state around a crack ratio of 0.46.

Test 3 indicates that the LEFM assumptions made for plane strain and plane stress states are valid for crack lengths of up to 6.0 mm (0.5 crack ratio) and 6.8 mm (0.57 crack ratio) respectively (Fig. 16b). There is a greater improvement in the limiting crack size for the plane strain state than for the plane stress state. The next section discusses the observation that significant errors in prediction occur beyond the limiting crack size for the plane stress state.

5.3. Results and discussions

5.3.1. The crack propagation curve

This section demonstrates how the predicted results could represent the observed behaviour of the structure in the three tests. Firstly, the measured propagation curves were plotted over the predicted curves. The measured propagation curves for Tests 1 and 2 as well as the predicted curves are shown in Fig. 17a.

It can be noted that the predictions fitted the results reasonably well in Test 2. Test 1 had a slight bulge beyond a crack length of 7 mm, due to problems with fluctuations in the supply voltage. The problems were obviously exacerbated by the fact that the limit for the applicability of LEFM was exceeded at this crack size. The power supply unit was changed in the following tests.

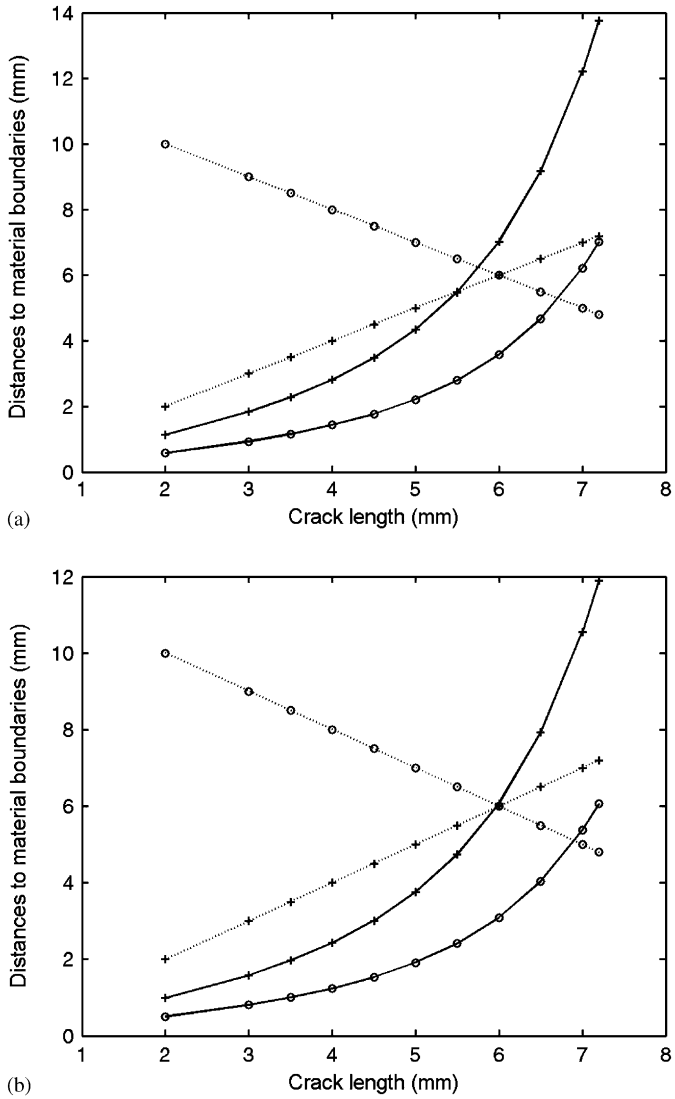

Fig. 16. Limits of applicability of LEFM—crack length (····+····), remaining material (····⊙····), plane strain limit (—+—) and plane stress limit (—⊙—). (a) Tests 1 and 2. (b) Test 3. As both t and h are large, they are disregarded.

In Test 3, the predictions showed a good correlation with the experimental results (Fig. 17b). However, the predictions at larger crack sizes were quite poor because of the violation of LEFM theory.

The remaining service life of the beams was determined from the propagation curves, as shown in Figs. 18a and b. The prediction errors plotted in Figs. 19a and b show that the prediction curve is able to approximate the remaining life to within a 40% error for crack ratios of less than 0.55. These errors illustrate only the accuracy of the FEM calculation according to LEFM. In all three tests, the results show that beyond this crack ratio it becomes extremely difficult to obtain accurate estimates for the remaining service life of a beam. This agrees with the calculated limits of crack sizes for the applicability of LEFM theory, as shown in Figs. 16a and b.

5.3.2. *Changes in acceleration response*

The FEM was used to calculate the acceleration responses for each damage scenario. These accelerations were filtered around the 7-Hz frequency of the excitation signal. Then the root mean square values of the accelerations were computed and plotted against the crack lengths. The trend in the plotted root mean square values shows an increase as the crack length increases.

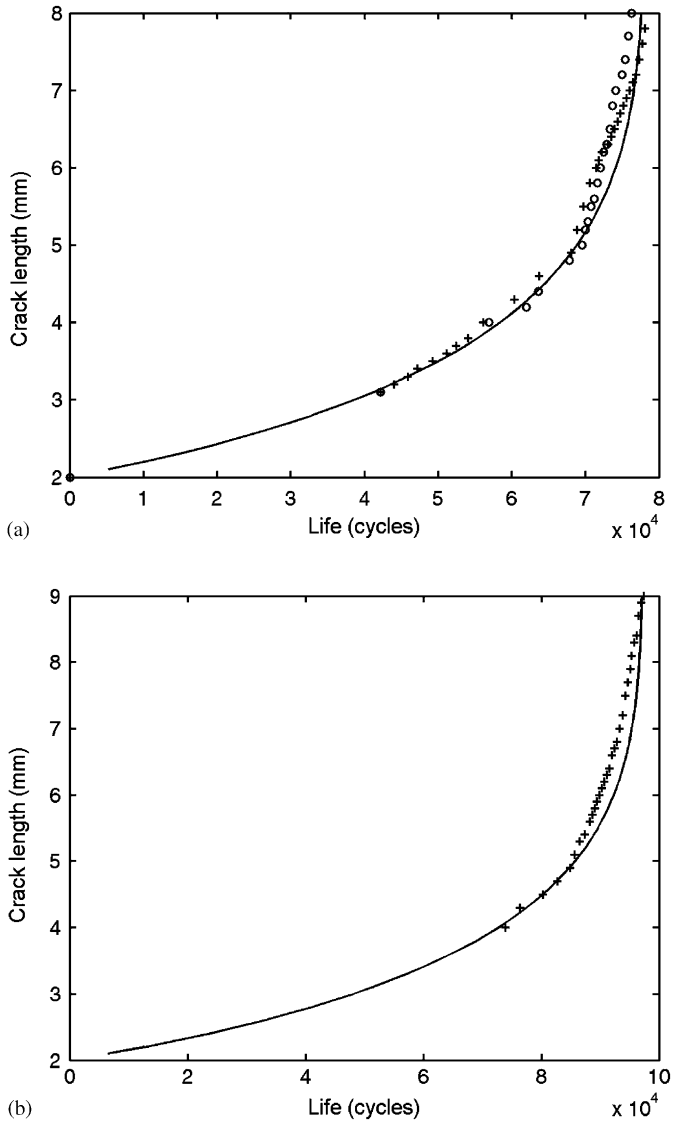

Fig. 17. Correspondence between measured and predicted (——) crack propagation lives: (a) Test 1 (+) and Test 2 (O) and (b) Test 3.

The root mean square values calculated from the measured data for each test were plotted over those from the values predicted by the model. The results show that Test 1 correlated fairly well at a number of crack lengths but correlated poorly around a crack length of 4 mm (Fig. 20a). This was due to loose screws, which eventually failed around that crack length. Fig. 20b shows that Test 2 correlated better with the predicted curve.

Test 3 shows there was a good correlation in the initial stages of crack growth, but that the correlation became very poor in the advanced stages (Fig. 20c) because the LEFM assumptions were severely violated at that stage.

5.3.3. Changes in χ_0^2 values

The χ_{0m}^2 values calculated from the measured data were plotted over the predictions χ_{0p}^2 obtained from the model. The results are shown in Figs. 21a, b and c. The plotted results show a good correlation between the experimental and predicted results, especially in Test 2, and for shorter crack sizes in Test 3. The above-mentioned problems with loose screws marred the performance of the predicted curve in Test 1.

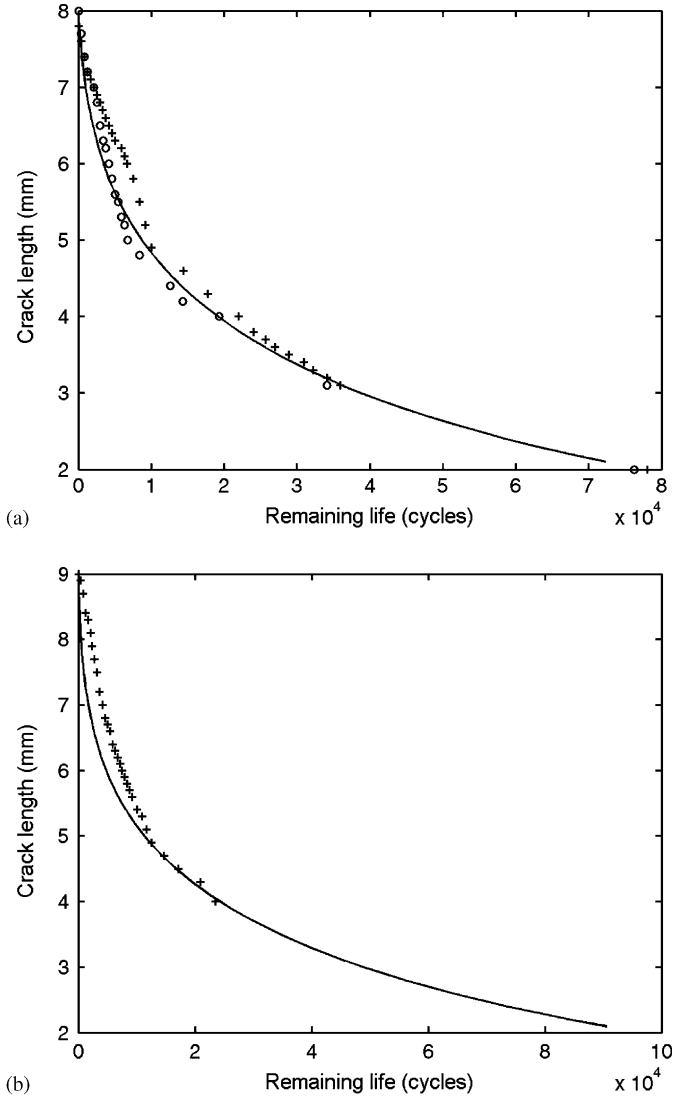

Fig. 18. Correspondence between measured and predicted (——) remaining service lives: (a) Test 1 (+) and Test 2 (O) and (b) Test 3.

The results obtained from the three tests show that with proper control over the physical set-up, accurate predictions can be made within the limits of LEFM theory. Therefore, as long as the crack length has not grown beyond this limit, the proposed technique is capable of estimating the crack length and the remaining service life of a beam within an error margin of 40%.

It was noted that after using the FEM for calculating the time responses, the rest of the process required little computational effort. For example, determining both the propagation life curve and the χ^2_{0m} value curve for each test took 106 s on a Pentium 4 personal computer with 1.7 GHz and 256 MB of random access memory. Each test consisted of 32 selected responses where each response signal contained 12 000 data units. Therefore it would take a far shorter time to process a single measured response signal.

6. Conclusion

A technique based on finite element simulation and operational time response monitoring has been shown to provide a complete identification of structural damage. The technique involves the finite element modelling

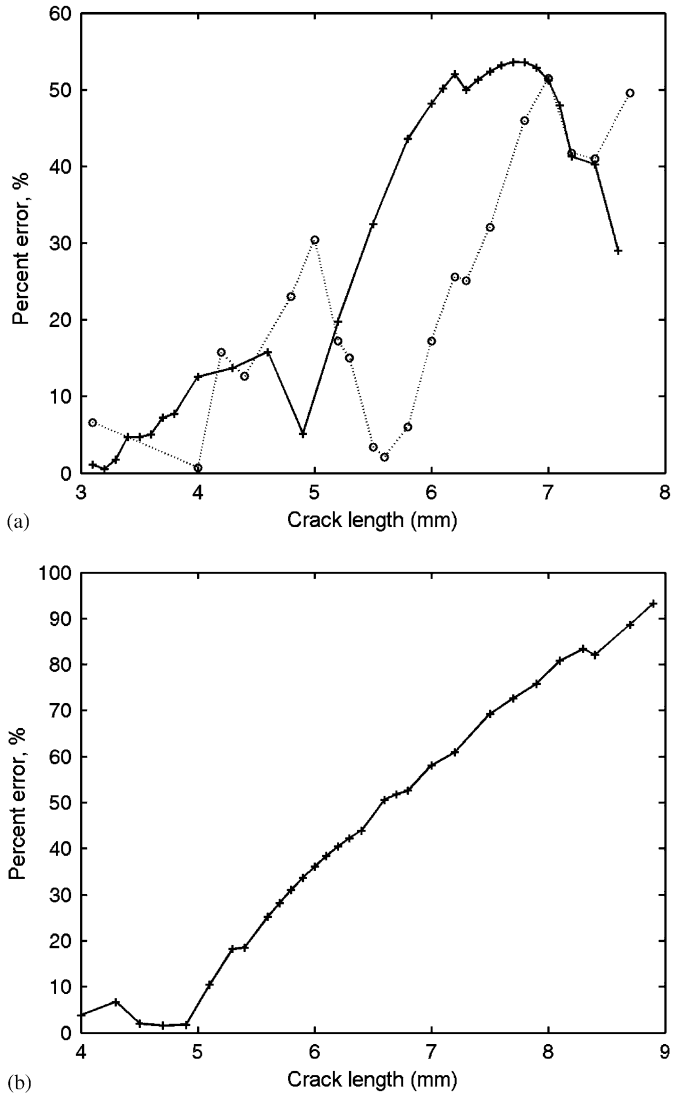

Fig. 19. Prediction errors of remaining service life: (a) Test 1 (—+—) and Test 2 (····⊙····) and (b) Test 3.

of the structural system from which a multivariable state-space model is identified. The multivariable state-space model is inverted using time-domain-based techniques so that operational forces can be determined. The calculated operational forces are applied to the structural FEM to identify high stress spots on the real structure.

The new technique identifies Level 1 by using changes in the measured operational responses via test statistic values. The test statistics are compared with a threshold value which is calculated at 1% of undamaged structure's response. The mere change in the value of the test statistics from this threshold value is considered to indicate the presence of structural damage.

Level 2 is identified through the locations of stress hot spots on the structural FEM. It is expected that these hot spots are the most likely damage locations. This is considered conservative and probably more applicable with this technique where structural operational responses are used for damage identification. Since the main focus of the work was to extend on the existing methods to identify all the four levels, this was quite satisfactory.

In this technique, structural damage is modelled in terms of crack length to allow for the application of LEFM theory. Thus, several damage scenarios are input into the structural FEM in the identified damage

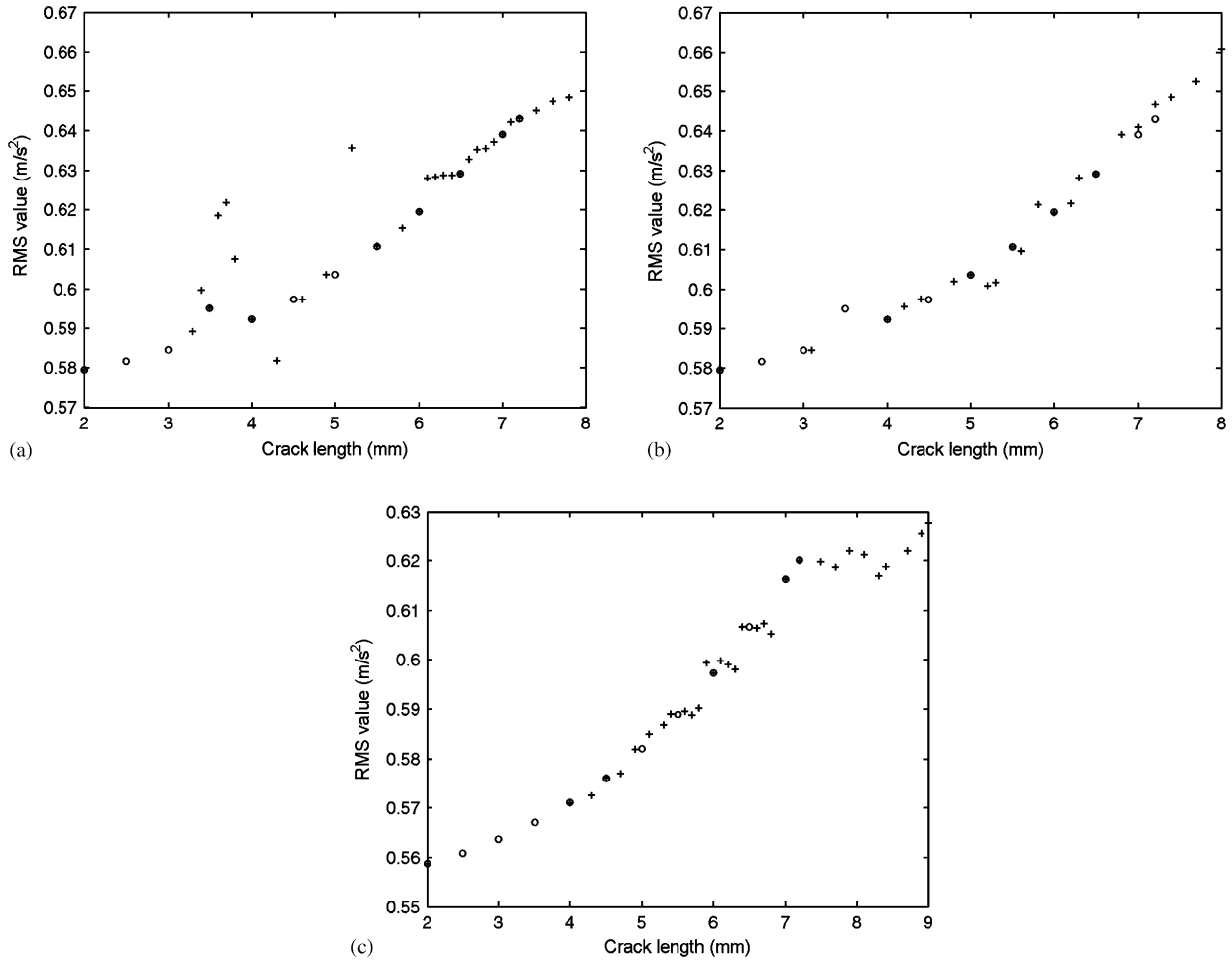

Fig. 20. Predicted (O) and measured (+) root mean square values: (a) Test 1, (b) Test 2 and (c) Test 3.

location. Then structural time responses are calculated for each scenario using FEM. The test statistic values are calculated for each damage scenario. Therefore, a test statistic value obtained from each measured response is compared with any of these calculated values to find its closest match. This identifies Level 3. Then the Paris law is used to predict remaining service life for each damage scenario. Thus having determined the severity of damage in Level 3, the corresponding remaining service life is simultaneously determined to identify Level 4.

The technique has been verified through numerical and experimental case studies. Through the numerical case study, it has been observed that more accurate estimates are obtainable by performing a sensitivity-based procedure, which minimizes an error between the measured response and a closest match to the predicted response. The results in both case studies show that the remaining life predictions at lower levels of structural damage are more accurate than at larger crack lengths.

The analysis on the experimental case study showed that the predictions were accurate to within an error margin of 40% for crack ratios of less than 0.55. This prediction error illustrates only the accuracy of the FEM calculation according to LEFM. Additional errors should be considered when estimating crack length by vibration measurements to illustrate the accuracy of the technique.

However, the results agreed with the observations on the limits of applicability of the LEFM theory. The limits of applicability of LEFM theory were noted to lie between the crack ratios of 0.55 and 0.6. Since it was also observed that the crack grew very rapidly beyond this limit, it could be considered as the transition region

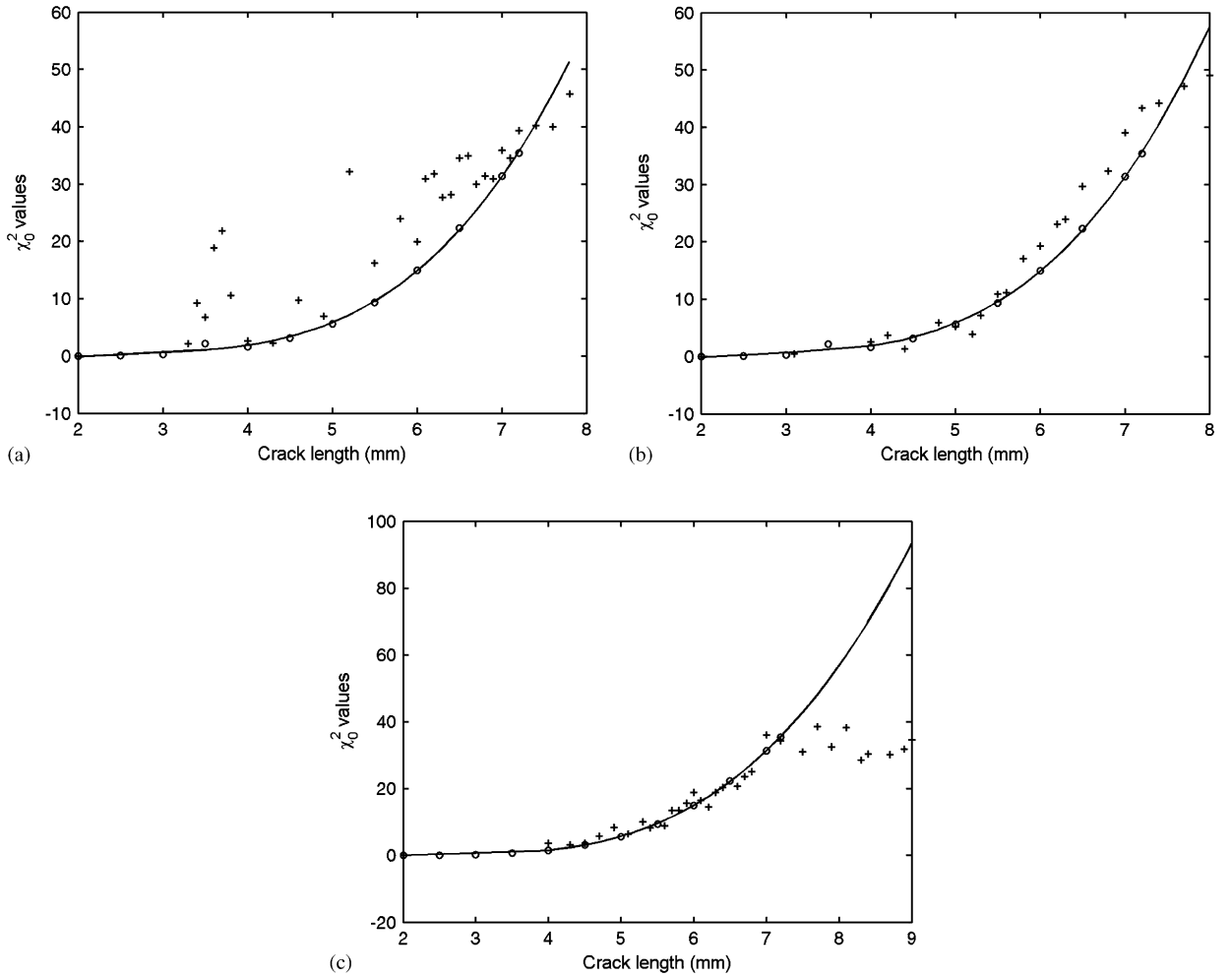

Fig. 21. Fit between predicted (O) and measured (+) test statistic values: (a) Test 1, (b) Test 2 and (c) Test 3.

into unstable crack growth phase. Therefore, it can be concluded that the technique is capable of identifying the four levels of damage identification up to the crack ratio of 0.55.

The technique has the practical attraction of requiring less computational effort during the damage identification phase hence is suitable for continuous monitoring of structural health. A further advantage lies in its better sensitivity to structural damage than the popularly used method of frequency shift monitoring. Through the numerical study the proposed technique was shown to be over three times as much sensitive as the natural frequency shift technique. A further comparison of the relative changes in the damage sensitive features up to a crack ratio of 0.6, showed a minimum relative change of 30% for the proposed technique against a maximum relative change of 20% for the frequency shift technique.

It is important to note some precautionary measures in the application of the technique. Since the operational time responses are not a property of the structural system, there are a few factors which should be considered. Firstly, the FEM must be able to predict the measured responses accurately. The force levels must be properly controlled so that no substantial fluctuations occur. Finally, the boundary constraints, joints and couplings must remain in their designed functional state.

It might be recommended that in identifying Level 1, thorough investigation into the threshold value of the test statistic value be performed. In the present study purely numerical investigation was used but this could be further enhanced by an experimental study.

The location of damage is performed by identifying the high stress points on the structural FEM. In a more complex structure, there would be more hot spots which might make it difficult to quantify damage and determine remaining service life by the technique in its present state. If many hot spots appear it might be necessary to pinpoint those which are most influential in causing the changes in the test statistics through a sensitivity-based procedure or to reduce the damage condition into an equivalent single damage scenario. However, the problem with this might be how to combine the different damage scenarios arising from many hot spots into a single equivalent damage scenario so that Levels 3 and 4 could be identified.

Besides, practical structures may pose other problems like varying boundary conditions and joints. The present technique may identify a change in the boundary conditions and joints as a potential damage location. Thus, this situation might raise similar problems to cases of occurrence of many hot spots that are already discussed. However, these problems might be recommended for further investigations.

The technique could prove to be useful for complete identification of damage in structures like bridges, telegraph towers and long suspension systems where sensitivity is a real problem. In the present technique, a homogeneous structure was studied. Therefore, for further study, I recommend that a more practical non-homogenous or composite structure be studied. This might result in changes in some of the applied concepts (like the LEFM, particularly the Paris law) although the fundamental procedure may remain the same. It would be interesting to note how other structural damage concepts would work with the procedure compared to the present one.

Other important areas for future study may include investigation into development of the technique under extreme load varying operating conditions. In the technique's present state, it may be applicable to very limited and highly controlled (e.g. laboratory) situations. But in most practical structural systems, the load levels are random in nature. In addition, attention was given to the open mode of fracture (bending only or mode I of fracture). Practical structures may not strictly fracture in this mode only. Therefore, it might be necessary to consider developing techniques for other modes of fracture or their combinations. As a result, techniques for identification of branched crack geometries may be developed.

References

[1] A. Rytter, Vibration-based Inspection of Civil Engineering Structures, PhD Thesis, Aalborg University, 1993.
[2] S.W. Doebling, C.R. Farrar, M.B. Prime, D.W. Shevitz, Damage identification and health monitoring of structural and mechanical systems from changes in their vibration characteristics: a literature review, Los Alamos National Laboratory Report LA-13070-MS, UC-900, 1996.
[3] C.R. Farrar, S.W. Doebling, An overview of modal-based damage detection identification methods. Engineering Analysis Group, Los Alamos National Laboratory, New Mexico, 1997.
[4] C.R. Farrar, S.W. Doebling, T.A. Duffey, Vibration-based damage detection, Los Alamos National Laboratory MS P-946, 1997.
[5] M.J. Bement, C.R. Farrar, Issues for the application of statistical models in damage detection, *Proceedings of the 18th International Modal Analysis Conference*, San Antonio, Texas, 2000.
[6] J.B. Bodeux, J.C. Golinval, Modal identification and damage detection using the data-driven stochastic subspace and ARMAV methods, *Mechanical Systems and Signal Processing* 17 (1) (2003) 83–89.
[7] A. Raich, T. Liszkai, A model parameter updating damage detection technique using genetic algorithm, in: K. Jârmai, J. Farkas (Eds.), *Metal Structures—Design, Fabrication, Economy*, Millpress, Rotterdam, 2003.
[8] H. Sohn, C.R. Farrar, Damage diagnosis using time series analysis of vibration signals, *Journal of Smart Materials and Structures* 10 (2001) 1–6.
[9] H. Sohn, M.L. Fugate, C.R. Farrar, Continuous structural monitoring using statistical process control, *Proceedings of the 18th International Modal Analysis Conference*, San Antonio, Texas, 2000.
[10] K. Worden, G. Manson, N.R.J. Fieller, Damage detection using outlier analysis, *Journal of Sound and Vibration* 229 (3) (2000) 647–667.
[11] K. Worden, G. Manson, D. Allman, Experimental validation of a health monitoring methodology—part I: novelty detection on a laboratory structure, *Journal of Sound and Vibration* 259 (2) (2003) 323–343.
[12] K. Worden, G. Manson, D. Allman, Experimental validation of a health monitoring methodology—part II: novelty detection on a gnat aircraft, *Journal of Sound and Vibration* 259 (2) (2003) 345–363.
[13] J.L. Zapico, M.P. Gonzâlez, K. Worden, Damage assessment using neural networks, *Mechanical Systems and Signal Processing* 17 (1) (2003) 119–125.
[14] A.D. Raath, Structural Dynamic Response Reconstruction in the Time Domain, PhD Thesis, University of Pretoria, 1992.
[15] D.J. Ewins, *Modal Testing: Theory and Practice*, Research Studies Press Ltd., England, 1988.
[16] M. Krawczuk, A. Żak, W. Ostachowicz, Elastic beam finite element with a transverse elasto-plastic crack, *Finite Element in Analysis and Design* 34 (2000) 61–73.

[17] R.T. Haftka, Z. Gürdal, M.P. Kamat, *Elements of Structural Optimisation*, Kluwer Academic Publishers, Dordrecht, 1990.
[18] D.C. Montgomery, *Design and Analysis of Experiments*, Wiley, New York, 1996.
[19] J.A. Bannantine, J.J. Comer, J.L. Handrock, *Fundamentals of Metal Fatigue Analysis*, Prentice-Hall Inc., Englewood Cliffs, NJ, 1990.
[20] N.E. Dowling, *Mechanical Behaviour of Materials: Engineering Methods for Deformation, Fracture and Fatigue*, Prentice-Hall Inc., Englewood Cliffs, NJ, 1999.
[21] S.S. Rao, *Mechanical Vibrations*, Addison-Wesley Publishing Company, New York, 1995.
[22] J.E. Shigley, C.R. Mischke, R.G. Budynas, *Mechanical Engineering Design*, McGraw Hill Higher Education, New York, 2003.
[23] Strain gauges and accessories catalog, HBM, Germany.